



Mo-doped CoP nanosheets as high-performance electrocatalyst for HER and OER

Shimin Li^{1,2} · Lei Bai^{1,2} · Haibiao Shi¹ · Xianfeng Hao¹ · Ling Chen¹ · Xiujuan Qin^{1,2} · Guangjie Shao^{1,2}

Received: 15 December 2020 / Revised: 31 March 2021 / Accepted: 21 April 2021 / Published online: 5 May 2021
© The Author(s), under exclusive licence to Springer-Verlag GmbH Germany, part of Springer Nature 2021

Abstract

Transition-metal doping and structural improvement are facile and feasible strategies to obtain highly active catalysts for hydrogen evolution reaction (HER) and oxygen evolution reaction (OER). Herein, we prepare Mo-CoP with a nanosheet structure via hydrothermal reactions and phosphorization. Taking advantage of the nanosheet array, the good electrocatalytic performance of Co-based materials for HER and excellent performance of Co-based phosphide for OER are fully demonstrated. Mo-CoP requires only 112 and 329.9 mV to achieve a current density of 100 mA/cm² for HER and OER in 1.0 M KOH, respectively. Furthermore, when it was used as bifunctional electrocatalyst, Mo-CoP could deliver 10 mA/cm² at a low cell voltage of 1.54 V. It was found that the activity of Mo-CoP could be ascribed to the structure of nanosheet and the synergistic role of two different metal phosphides. The most important is that the introduction of Mo improves the activity of the catalyst.

Keywords Mo-CoP · Electrocatalyst · HER · OER · Overall water splitting

Introduction

Hydrogen fuel, as a sort of environmentally friendly resource which could displace the status of conventional fossil fuel, is of paramount significance for sustainable development and environmental protection [1]. Among various hydrogen production strategies, water electrolysis, a kind of clean and cost-effective strategy, had aroused gigantic attention due to its feasibility and sustainability [2, 3]. As a part of the reaction of the water splitting system, hydrogen evolution reaction (HER) which

proceeds in two steps had caught intense attention [4, 5]. Owing to their splendid kinetics for enhancing the HER and their negligible overpotentials (η), Pt-based materials are thought to be state-of-the-art electrocatalysts [6, 7]. Additionally, oxygen evolution reaction (OER) is also an indispensable and vital part of the process of overall water splitting [8]. Owing to the complicated four proton-coupled electron transfer (PCET) steps, OER is harder to achieve those steps than HER [9]. To date, Ru-/Ir-based materials are regarded as the most efficient catalysts toward OER [10]. Unfortunately, to a large extent, the scarcity and high-cost production of both Pt-based and Ru-/Ir-based electrocatalysts seriously impede their large-scale practical applications [11]. For these reasons mentioned above, it is highly imperative to design electrocatalysts based on earth-abundant materials to replace those noble-metals-based electrocatalysts.

Recently, the efficient electrocatalysts with environmental benignity for water splitting have caught intense attention, such as metal alloys [12, 13], phosphides [14, 15], sulfides [16, 17], nitrides [18, 19], and carbides [20]. Among these materials, transition-metal phosphides (TMPs) show palmary catalytic capabilities owing to the oxidation state changes of those transition metals. In addition, owing to its long-term stability, TMP is a suitable substitute for precious metal materials because of its good wettability and stability [19]. As a

✉ Xianfeng Hao
xfhao@ysu.edu.cn

✉ Ling Chen
hhchen@ysu.edu.cn

✉ Xiujuan Qin
qinxj@ysu.edu.cn

✉ Guangjie Shao
shaoguangjie@ysu.edu.cn

¹ Hebei Key Laboratory of Heavy Metal Deep-Remediation in Water and Resource Reuse, College of Environmental and Chemical Engineering, Yanshan University, Qinhuangdao 066004, China

² State Key Laboratory of Metastable Materials Science and Technology, Yanshan University, Qinhuangdao 066004, China

transition metal, Co is regarded as one promising raw material to synthesize the efficient catalysts for water splitting because its facile oxidation state changes [21]. Therefore, CoP which has caught the intense attention of many researchers was regarded as an outstanding catalyst for water splitting. Therefore, CoP in a variety of morphologies was investigated for HER and OER, including nanosheet [22], nanowire [23], and nanotube [24]. Liu and co-workers reported self-standing CoP nanosheet (CoP NA/CC) array promoted HER and OER in alkaline media with good activity [25]. For overall water splitting, the catalysts reach 10 mA/cm^2 with 1.65 V in 1.0 M KOH. Additionally, Zhang and co-workers obtained CoP nanowires via anion-exchange and phosphating process [23]. Despite having good performance for water splitting, the stability of CoP nanowire they reported is not as good as CoP nanosheets. CoP nanotubes have also been designed via an organic solvent-free method [24], but the catalyst, without a template, is difficult to be prepared.

In addition, incorporation of metallic (e.g., Al) and nonmetallic elements (e.g., N) into Co-based catalysts had been confirmed to improve catalytic activities; in the work of Zhang, Al-doped CoP nanoarray was synthesized to improve the effectiveness of water splitting, manifesting that the introduction of Al could enhance the activity of CoP [26]. Furthermore, Mo-doped cobalt phosphide nanosheets with exceptional activity for HER were successfully prepared on carbon cloth [27], while its performance toward OER has not been discussed in detail. Besides, in the study of Liu and co-workers, with N incorporation, the nitrogen-doped CoP nanoarray exhibits higher HER activity than CoP due to the amount of available active sites that increased obviously, and the intrinsic catalytic activity was promoted [28].

In light of such motivation, we design an efficient bifunctional electrocatalyst for overall water splitting. Herein, we take an easily manipulated and efficient method to prepare efficient and stable Mo-doped CoP nanosheets on nickel foam (Mo-CoP). The introduction of Mo not only could improve the structure of the catalyst but could also enhance the activity. This approach substantially optimizes the surface area of the catalyst, thus leading to outstanding activity. During the second hydrothermal process, Mo ions imbedded in the CoCO nanosheets to form abundant Mo-Co interface sites. After calcining with NaH_2PO_2 , two different metal phosphides were formed. As a result, the as-prepared material delivers a current density of 100 mA/cm^2 at overpotentials of 112 mV for HER and 329.9 mV for OER in 1.0 M KOH. Besides, Mo-CoP catalyst showed high durability under alkaline electrolytes. When used as bifunctional electrocatalyst, Mo-CoP could deliver 10 mA/cm^2 at a low cell voltage of 1.54 V. This work offers a facile methodology for the development of a heterojunction catalyst.

Experimental section

Synthesis of Mo-CoP nanosheets on nickel foam

In a typical synthesis, $\text{Co}(\text{NO})_3 \cdot 6\text{H}_2\text{O}$ (3.33 mmol), NH_4F (13.33 mmol), and urea (16.67 mmol) were dissolved in 60-mL distilled water. After that, the as-prepared solution was transferred into a 100-mL autoclave with one piece of clean nickel foam ($1 \times 6 \text{ cm}^2$). Secondly, the autoclave was sealed and heated at 100°C for 6 h. After cooling to room temperature, the samples were taken out, and then they were rinsed and dried. In order to synthesize CoMoO_4 , 0.4 mmol of Na_2MoO_4 was dissolved in 30 mL of distilled water. After that, the as-prepared solution was transferred to a 100-mL autoclave with one piece of nickel foam covered with CoCO. Thereafter, the autoclave was sealed and heated at 140°C for 6 h. After cooling to room temperature, the samples were taken out, and then they were rinsed and dried. In order to synthesize Mo-CoP, CoMoO_4 and NaH_2PO_2 were put at two different positions with NaH_2PO_2 of 1 g at the upstream side of the tube furnace. Subsequently, the samples were heated at 350°C with 2°C/min and kept for 2 h under argon flow, and then cooled to room temperature. The calculated area mass loading of NF ($10 \times 10 \text{ mm}^2$) was calculated to be 0.0168 g.

Synthesis of Mo-CoP nanosheets with different proportions (Mo-CoP-x) on Nickel Foam

In order to synthesize Mo-CoP-x, 0.2, 0.6, and 0.8 mmol Na_2MoO_4 were dissolved in 30 mL of distilled water respectively. After that, the as-prepared solution was transferred to three 100-mL autoclaves where there is one piece of nickel foam covered with CoCO. Thereafter, the autoclave was sealed and heated at 140°C for 6 h; CoMoO_{4-x} ($x = 0.2, 0.6, \text{ and } 0.8$) was obtained. Finally, CoMoO_{4-x} is processed through the same phosphating process to obtain Mo-CoP-x.

Synthesis of pure CoP nanosheet array on Nickel foam

In order to synthesize pure CoP, CoCO and NaH_2PO_2 were put at two different positions with NaH_2PO_2 of 1 g at the upstream side of the tube furnace. The other reaction conditions are the same as those of Mo-CoP.

Physical characterization

XRD patterns of as-prepared materials were performed on a Rigaku Smart Lab X-ray diffractometer operated at 40 kV using $\text{Cu } \alpha$ radiation source at a scan rate of 5° . The morphology of as-prepared samples was characterized by field emission scanning electron microscopy (FESEM, Zeiss Supra 55) with an accelerating voltage of 15 kV and a

transmission electron microscope (TEM) with an accelerating voltage of 100 kV. X-ray photoelectron spectroscopy (XPS) with a Kratos XSAM-800 spectrometer was used to investigate the valence state of the elements.

Electrochemical measurements

Electrochemical measurements were carried out in a typical three-electrode cell with a CHI 660E electrochemical workstation (CH Instruments, Inc., Shanghai) at room temperature ($\sim 25^\circ\text{C}$) in 1 M KOH. The Mo-CoP (10 mm \times 10 mm), Pt foil (10 mm \times 10 mm), and Hg/HgO electrode are used as working electrode, counter electrode, and reference electrode, respectively. The polarization curves of HER and OER were obtained at a scan rate of 1.0 mV/s in 1.0 M KOH at room temperature. All the potentials were calibrated to a reversible hydrogen electrode (RHE) by the formula E (vs RHE) = E (vs Hg/HgO) + 0.059 \times pH + 0.0977 V. For comparison, the electrocatalytic performance of NF, Pt/C, and other related electrodes were tested. Electrochemical impedance spectroscopy (EIS) measurements were performed in the frequency range of 0.01– 10^5 Hz with a 5-mV AC voltage amplitude at different potentials (125 mV for HER and 250 mV for OER). The durability test was performed for 12 h at a current density of 50 mA/cm². To calculate the electrochemically active surface area (ECSA), the double-layer capacitance (C_{dl}) is calculated from the cyclic voltammetry (CV) which is performed at varied scan rates in the potential range of 0.1–0.2 V (vs RHE).

Result and discussion

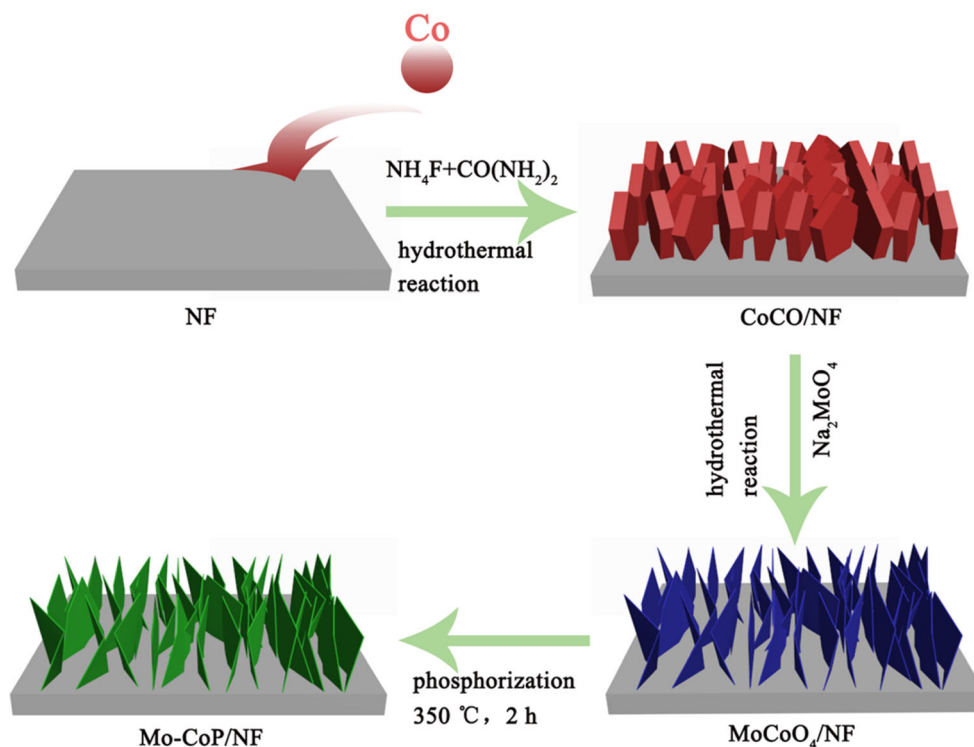
Scheme 1 visually depicts the entire process of catalyst production and the changes on the surface of NF during the process. The Mo-doped CoP nanosheet arrays were successfully grown on NF by hydrothermal and phosphidation procedure. Additionally, the corresponding morphology changes from CoCO to CoMoO₄ were revealed via the SEM images in Fig. 1. At first, NF which could provide a three-dimensional (3D) skeleton was used as a substrate to fabricate two-dimensional (2D) CoCO via hydrothermal reaction (Fig. 1a). As shown in Fig. 1b, quite a few nanosheets of uneven thickness dispersed on NF irregularly, CoMoO₄ nanosheet array was obtained after the second hydrothermal reaction, and the thickness of the nanosheets on NF decreased obviously. From Figure S1, the thickness of CoMoO₄ nanosheet is about 20 nm. The as-prepared CoMoO₄ was used as the template to synthesize the Mo-CoP via phosphidating and the nanosheet structure of the precursor was preserved intact. Meanwhile, compared with CoMoO₄ nanosheets, the surface of Mo-CoP nanosheets is rougher than those of CoMoO₄. And the top view of NF, CoCO, CoMoO₄, and Mo-CoP strongly proves that the prepared material is uniformly distributed on the

surface of NF (Figure S2). Besides, the EDS element mappings of Mo-CoP (Figure S3) further exhibit a uniform distribution of Co, Mo, and P throughout the structure. Furthermore, from the EDS spectrums of Mo-CoP (Figure S4), the atomic ratio of Mo: Co: P is 1.27 : 6.9 : 10.91. As depicted in Figure S5, the surface of CoP is covered by an array of nanorods, and Co and P are evenly distributed on the CoP surface. In addition, the atomic ratio of Co: P is 25.37: 19.88 (Figure S6).

In order to study the effect of reaction time on the morphology of Mo-CoP, some samples were synthesized at 140 °C for different reaction time. In Fig. 2a, after treating with Na₂MoO₄ at 140 °C for 2 h and then calcined with NaH₂PO₂, the nanosheets disappeared, and many irregular nanosheets are shrouded above the nanowires. As the reaction time is prolonged to 4 h, the nanowires are completely converted into a regular nanosheets array (Fig. 2b), but the surface of the nanosheets is so smooth that it will not be conducive to the display of the active site. When the reaction time is prolonged to 6 h, the nanosheet array obtained is cruder (Fig. 2c). However, as the reaction time prolonged to 8 h, the nanosheet array is destroyed (Fig. 2d). Set the reaction time to 6 h, and the structure of the material will be more conducive to the diffusion of electrolyte and the precipitation of gas.

For the electrocatalytic activity is sensitive to the valence state and the coordination environment of metal centers, the X-ray photoelectron spectroscopy (XPS) of Mo-CoP was conducted to investigate the chemical composition and valence state of the elements on the surface of it. As shown in Figure S7, the survey spectrum manifests the existence of Co, Mo, and P. Figure 3a displays the Co 2p XPS spectrum, in which the peaks at 777.9 and 793.4 eV are attributed to Co 2p_{3/2} and 2p_{1/2}, demonstrating the presence of the Co⁰. The peaks of Co 2p_{3/2} and 2p_{1/2} appear at 782.3 and 798.2 eV, respectively, demonstrating the presence of the Co²⁺ species in the Mo-CoP [29–31]. Additionally, the peaks at 787.0 and 802.8 eV could be ascribed to the charge-transfer satellite structure. Figure 3b shows the XPS spectrum in the P 2p region, the peak at 134.4 eV belongs to the P-O. And the peaks at 129.8 and 129.1 eV could be ascribed to P 2p_{1/2} and P 2p_{3/2}, respectively, demonstrating the presence of Mo-P or Co-P in the metal phosphide. In the XPS spectrum of Mo 3d (Fig. 3c), the peaks at 232.61 (3d_{5/2}) and 235.39 eV (3d_{3/2}) could be ascribed to the oxidized Mo species (MoO₃) resulting from the surface oxidation of Mo-CoP, and the two peaks at 230.47 (Mo 3d_{5/2}) and 233.67 eV (Mo 3d_{3/2}) could be ascribed to Mo⁵⁺ [32]. Sodium hypophosphite generates reducing phosphine during the calcination process, which is one of the reasons for the existence of Co⁰ and Mo⁵⁺. For comparison, the XPS data of CoP was shown as well. The survey spectrum of CoP (Figure S8) manifests the presence of Co and P. Compared with Mo-CoP, in the high-magnification

Scheme 1 Synthetic procedure of Mo-CoP/NF



XPS spectra of CoP (Fig. 3d), the chemical states of Co and P are different from those of Mo-CoP. The binding energy of Co 2p of CoP at 778.7 (Co 2p_{3/2}), 782.2 (Co 2p_{3/2}), 792.9 (Co 2p_{1/2}), and 798.4 eV (Co 2p_{1/2}) shifts toward higher binding energies compared with that of Co 2p of Mo-CoP. Mo doping enhances the interaction between Co and P so that the binding

energy of Co decreases. Figure 3e shows the XPS spectrum in the P 2p region, and the binding energy of P 2p of CoP at 129.3 and 130.0 eV shifts toward higher binding energies compared with P 2p of Mo-CoP as well. The change in binding energy indicates that the charge is redistributed. The redistribution could be ascribed to the strong interaction between

Fig. 1 SEM images of NF (a), CoCO (b), CoMoO₄ (c), and Mo-CoP (d)

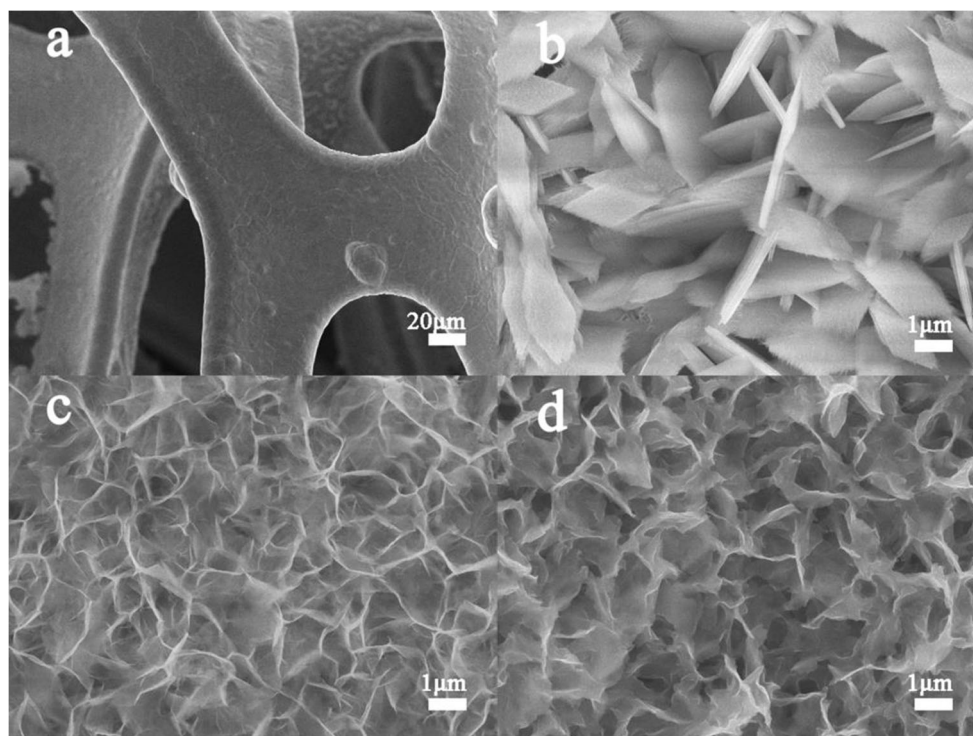
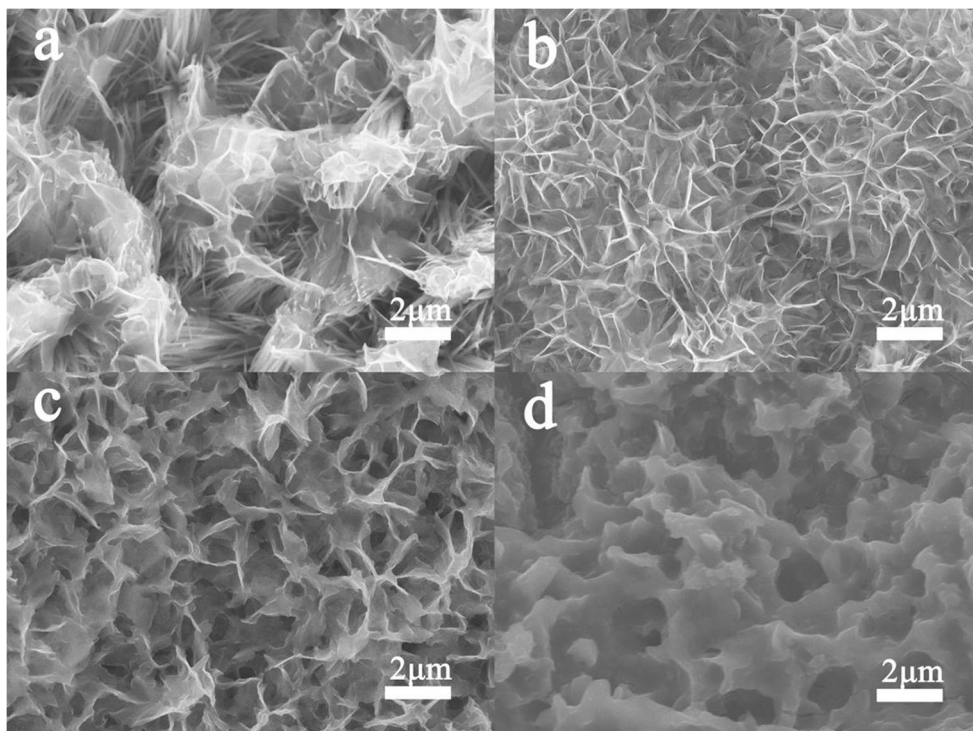


Fig. 2 SEM images of the CoCO reacted with Na₂MoO₄ at 140 °C for 2 h (a), 4 h (b), 6 h (c), and 8 h (d)



the interfaces of CoP and CoMoP [33] which could significantly improve the electrocatalytic activity.

The XRD patterns were recorded to figure out the crystallographic information of precursors and as-prepared catalysts. In Figure S9, XRD patterns of the samples confirm the

formation of CoCO and CoMoO₄. Among them, the XRD pattern of CoCO could be well indexed to Cobalt Oxalate Hydrate (JCPDS 25-0250). The emerging new peaks after the reaction with the Na₂MoO₄ can be attributed to CoMoO₄ (JCPDS 16-0309) and basic cobalt carbonate (JCPDS 48-

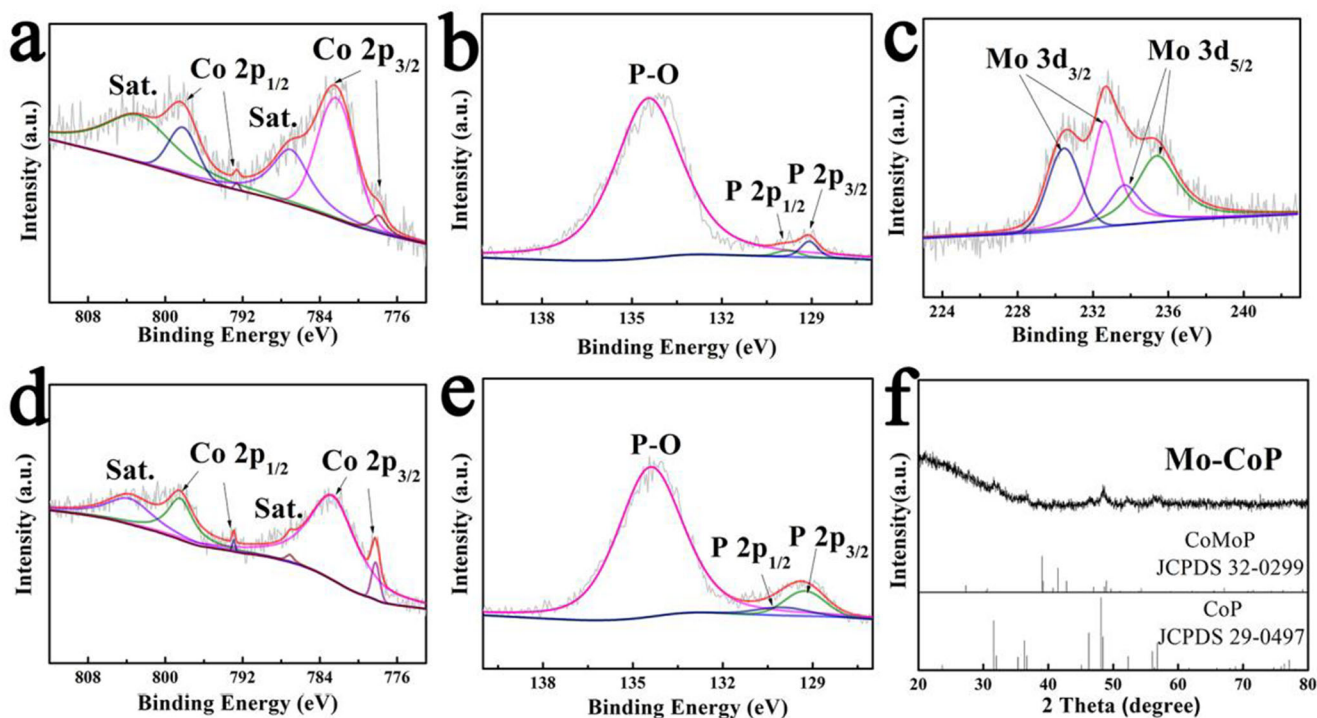


Fig. 3 High-magnification XPS spectra of Mo-CoP: Co 2p (a) P 2p (b), and Mo 3d (c); high-magnification XPS spectra of CoP: Co 2p (d) P 2p (e), and the XRD patterns of Mo-CoP (f)

0083), which could confirm that the CoCO is partially converted to CoMoO₄, mostly by hydrothermal reaction into basic cobalt carbonate (JCPDS 48-0083). As shown in Figure S10, the XRD pattern of precursor changes dramatically after phosphating. The new peaks at 31.60°, 36.32°, and 48.12° corresponding to (011), (111), and (211) planes of orthorhombic CoP (JCPDS 29-0497) in CoCO were converted to CoP after phosphating. The XRD pattern of Mo-CoP (Fig. 3f) could be well indexed to the orthorhombic CoP (JCPDS 29-0497), and the other peaks at 39.13°, 39.28°, 41.57°, and 42.87° could be ascribed to the (112), (210), (211), and (103) planes of orthorhombic CoMoP (JCPDS 32-0299), respectively. Mo-CoP is composed of CoMoP and CoP.

The electrocatalytic HER performance of Mo-CoP was evaluated. Additionally, CoMoO₄, CoP, Pt/C, and NF electrodes were also investigated. As shown in Fig. 4a and b, Mo-CoP electrode delivers high HER performance that could deliver 100 mA/cm² with a low overpotential of 112 mV which is much smaller than CoMoO₄ (η_{100} = 213.5 mV), CoP (η_{100} = 187.8 mV), and NF (η_{100} = 380.4 mV), and even close to that of the benchmark Pt/C (η_{100} = 99.7 mV). Figure 4b shows the overpotential of Mo-CoP and other references at the current density of 100 mA/cm². Comparing Figure S11 with S12, it is not difficult to find that phosphating reshapes the morphology of CoCO, and the structure of the material is transformed from a nanoplate array to a nanorod array. Although the CoMoO₄ obtained after reacting with Na₂MoO₄ was sufficiently improved in terms of morphology, the inherent activity of the material still needs to be improved. From the TEM image

(Figure S13), it is not difficult to find that the nanosheets on the surface of CoMoO₄ are too thin to be broken during the ultrasonic treatment, even after phosphating, which indicates that there are ultra-thin nanosheets on the surface of Mo-CoP. The improvement of morphology and the synergy between different phosphides are the main reasons for the distinctive activity of Mo-CoP. Besides, comparing with other Co-based electrocatalysts (Table S1 [34–40]), Mo-CoP is not inferior in terms of electrochemical performance. Combined with the structure of the catalyst, the reason for its distinctive performance should be ascribed to the 2D structure.

The Tafel plots of catalysts are shown in Fig. 4c. Mo-CoP possesses a Tafel slope of 69.1 mV/dec which is lower than that of CoMoO₄ (161.5 mV/dec), CoP (106.3 mV/dec), and NF (126.7 mV/dec). Typically, the Tafel slope is used to identify the kinetic process of electrochemical reactions. There are three kinds of reactions involved in HER: the Volmer, Heyrovsky, and Tafel reactions [41]. The Volmer reaction represents the initial electron transfer process and corresponds to the slope value of 30 mV/dec. The Heyrovsky reaction belongs to the electrochemical desorption step and corresponds to the slope value of 40 mV/dec. The Tafel reaction represents the compound desorption process and corresponds to the slope value of 120 mV/dec. Therefore, there are two feasible reaction ways for HER: Volmer-Heyrovsky and Volmer-Tafel. Herein, the Tafel slope of Mo-CoP is in the range of 40~120 mV/dec, indicating that the corresponding hydrogen evolution reaction takes in the Volmer-Heyrovsky pathway.

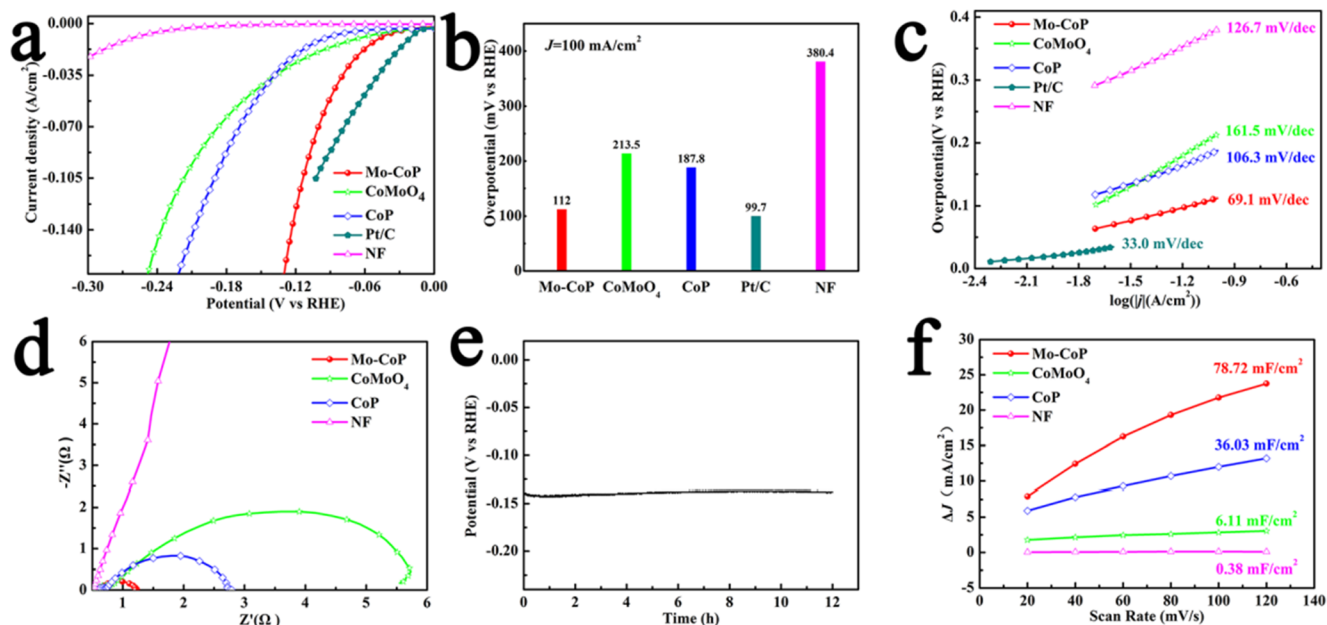


Fig. 4 a The HER polarization curves and of Mo-CoP, CoMoO₄, CoP, Pt/C, and NF. b The comparison of overpotential at 100 mA/cm² for Mo-CoP and other references. c The Tafel plots derived from (a). d Nyquist

plots of various catalysts. e Chronopotentiometry curve of Mo-CoP/NF was performed at geometric current densities of -50 mA/cm^2 . f C_{dl} of different electrodes

Additionally, charge-transfer resistance (R_{ct}) and electrochemical adsorption resistance (R_{ad}) were obtained by an equivalent circuit (Figure S14). As shown in the Nyquist plots (Figure 4d), Mo-CoP (0.5927 Ω) exhibits a smaller R_{ct} than CoMoO₄ (2.657 Ω) and NF (210.6 Ω). It is worth noting that R_{ad} of Mo-CoP is even lower than that of CoP, implying that the incorporation of molybdenum may accelerate electrochemical adsorption on the electrode surface which could be attributed to the nanosheet structure. During the second hydrothermal reaction, the morphology of the precursor changes from a thicker nanoplate array to a rougher nanosheet array, and the surface of the precursor becomes rougher. The morphology of the precursor was retained after phosphating, which makes it possible to expose more active sites. The morphology of the precursor is preserved after phosphating, which not only provides the possibility for more active sites to be exposed but also provides convenience for the full contact between the electrode and the electrolyte.

For studying the stability of Mo-CoP, chronopotentiometry was conducted at -50 mA/cm^2 for 12 h. In Fig. 4e, no conspicuous increase in the potential could be found, confirming that Mo-CoP has superior operational stability. As shown in Figure S15, after the test for 12 h, the *IR*-corrected polarization curves of Mo-CoP for HER had occurred a negative shift, indicating the improvement of the catalytic performance of the catalyst. In addition, comparing the SEM images before and after the durability test (Figure S16), it is not difficult to find that the nanosheet structure on the surface of the catalyst is well retained, which further illustrates the excellent stability of the catalyst.

The C_{dl} was also evaluated to investigate the electrochemical surface area (ECSA). Here, the C_{dl} is extracted from CV curves with different scan rates (20–120 mV/s) (Figure S17). The C_{dl} can be calculated by plotting the current density ΔJ ($\Delta J = J_a - J_c$, J_a is anodic current density, J_c is cathodic current density) against the scan rates, and half of the slope is C_{dl} . As shown in Fig. 4f, Mo-CoP exhibits a larger C_{dl} value of 78.70 mF/cm², almost 2.2-fold than that of CoP (36.03 mF/cm²) which confirmed that the introduction of Mo could improve the morphology and activity of the catalyst. Besides, the C_{dl} value of CoMoO₄ (6.11 mF/cm²) is less than eight-tenths of that of Mo-CoP which contributed to the fact that phosphating could increase the active sites of the catalysts. And these electrochemical tests demonstrated that the synergistic effect between CoP and CoMoP plays an important role in enhancing the catalytic activities.

The electrochemical OER activities of Mo-CoP, CoMoO₄, CoP, and NF were evaluated through cyclic voltammetry (CV). As shown in Fig. 5a, Mo-CoP exhibits the OER activity that reach 10 mA/cm² with a low overpotential of 269 mV, which outperforms those of CoP (280 mV), CoMoO₄ (291 mV), and NF (453 mV). And Mo-CoP exhibits better electrochemical kinetics than CoP and CoMoO₄. As shown in Fig.

5b, the Tafel slope of the Mo-CoP at approximately 86.8 mV/dec is smaller than that of CoMoO₄ (96.8 mV/dec) and CoP (87.6 mV/dec). It is worth noting that Mo-CoP outperforms many reported OER electrocatalysts (Table S2 [42–49]). And compared with other catalysts, the load transfer resistance of Mo-CoP is smaller (Fig. 5). Another thing worth mentioning is its good stability (Fig. 5d). After a 12-h durability test, the electrocatalytic oxygen evolution performance of the catalyst remained basically unchanged (Figure S18). Meanwhile, the morphology of the catalyst was completely destroyed after 12 h of durability test, which can be attributed to electrochemical remodeling (Figure S19).

In order to study the relationship between the concentration of sodium molybdate and the morphology and properties of the material, Mo-CoP-0.2, Mo-CoP-0.4, and Mo-CoP-0.8 were prepared. Mo-CoP exhibits much better electrocatalytic performance for HER (Figure S20) and OER (Figure S21). As shown in Figure S20a, the Mo-CoP obtained with 0.4 mol Na₂MoO₄ exhibits the lowest overpotential at 100 mA/cm² current densities compared to Mo-CoP-0.2, Mo-CoP-0.6, and Mo-CoP-0.8, indicating that the samples prepared with 0.4 mmol Na₂MoO₄ are the best. Meanwhile, as shown in Figure S20b, the Tafel slope of Mo-CoP is lower than that of Mo-CoP-0.2, Mo-CoP-0.6, and Mo-CoP-0.8. Otherwise, as described in Table S3 and Table S4, Mo-CoP possesses much lower charge-transfer resistance (0.5927 Ω) than Mo-CoP-0.2 (0.9967 Ω), Mo-CoP-0.6 (0.9139 Ω), and Mo-CoP-0.8 (1.245 Ω), which will help accelerate the progress of the electrochemical reaction. For OER, Mo-CoP exhibits much better electrocatalytic performance (Figure S21), which is possibly due to the rough nanosheet array, as revealed in the SEM images in Figure S21. As shown in Figure S21a, the Mo-CoP obtained with 0.4 mmol Na₂MoO₄ exhibits the lowest overpotential at 10 mA/cm² compared to Mo-CoP-0.2, Mo-CoP-0.6, and Mo-CoP-0.8. Meanwhile, Mo-CoP exhibits stronger electrochemical kinetics. As shown in Figure S21b, the Tafel slope of Mo-CoP is lower than those of Mo-CoP-0.2, Mo-CoP-0.6, and Mo-CoP-0.8, and such excellent electrochemical kinetics could improve the efficiency of the electrochemical reaction. As revealed in the SEM images in Figure S22, even if the concentration of Na₂MoO₄ is changed, the overall morphology of the catalyst is similar, but there are still differences in details. When the concentration of Na₂MoO₄ is 6.67 mM, as shown in Figure S22a, the nanosheet array is relatively sparse. When the concentration of Na₂MoO₄ is increased to 20 mM, as shown in Figure S22b, the nanosheet array is too dense, and this structure will not be conducive to electrolyte diffusion and gas precipitation. When the concentration of Na₂MoO₄ up to 26.67 mM, as shown in Figure S22d, some nanoplatelets cluster together to form a hill, and this structure will cause more active sites to be masked. However, when the amount of Na₂MoO₄ is 13.33 mM, the surface of the nanosheets is sufficiently rough and

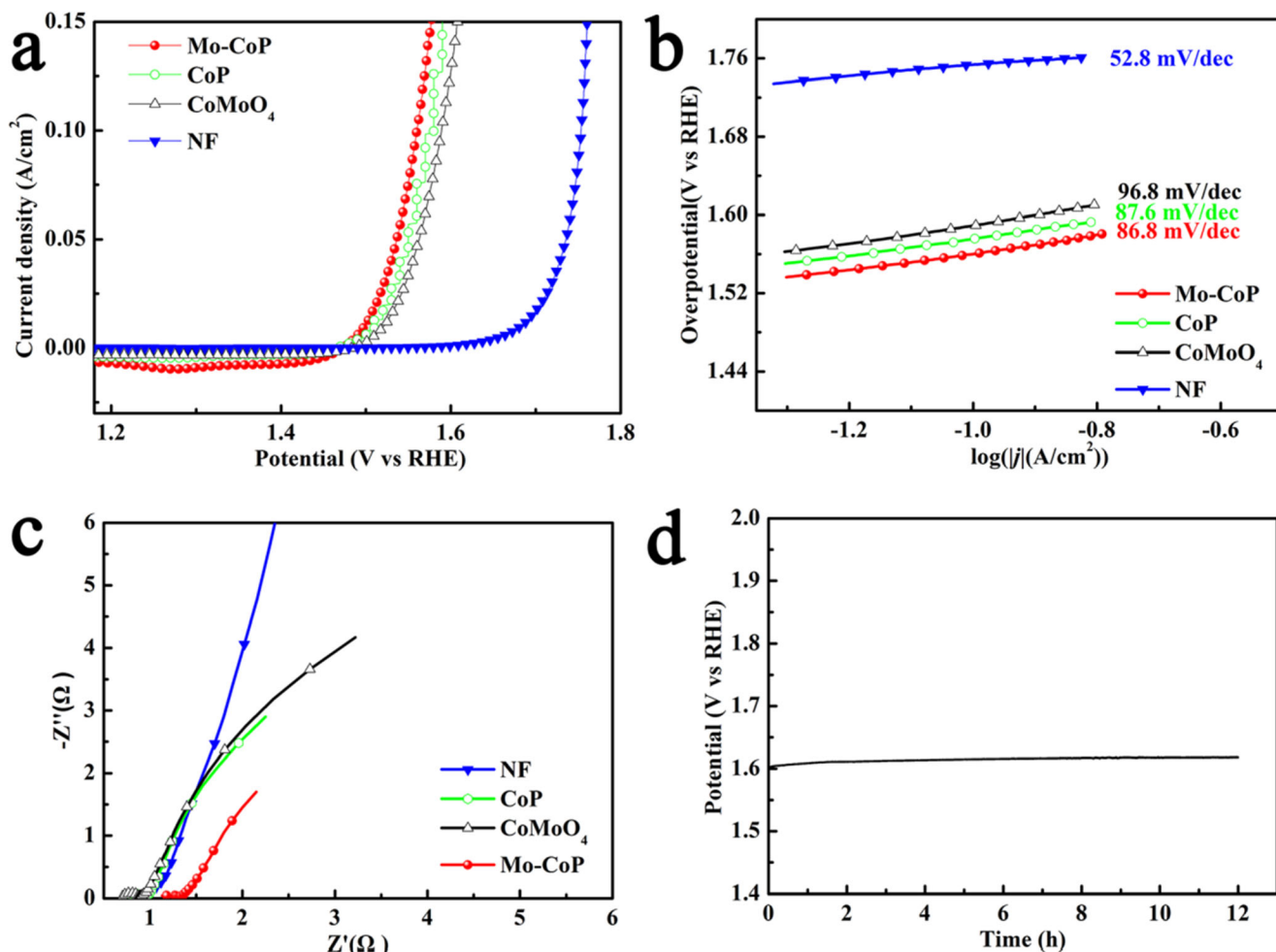


Fig. 5 Oxygen evolution reaction in 1 M KOH: **a** IR-corrected polarization curves for OER. **b** The Tafel plots derived from (a). **c** Nyquist plots of various catalysts with the fitting curves. **d** Chronopotentiometry curve of Mo-CoP/NF was performed at geometric current densities of 50 mA/cm^2

facilitates gas evolution. For electrocatalysts toward HER, the improvement of morphology is usually closely related to ECSA. As shown in Figure S23, Mo-CoP exhibits larger ECSA, and the ECSA of Mo-CoP-0.8 is larger than CoP, which further proves that the introduction of Mo could increase the active sites and improve the performance of the material.

Additionally, as shown in Figure S24 and S25, the reaction temperature during the second synthetic step also plays an important role in the electrocatalytic HER and OER activity of Mo-CoP. For HER, as shown in Figure S24a, the Mo-CoP obtained at 140°C exhibits the lowest overpotential at 100 mA/cm^2 compared to Mo-CoP-120 and Mo-CoP-160. Moreover, as shown in Figure S24b, the Tafel slope of Mo-CoP obtained at 140°C is lower than that of Mo-CoP-120 and Mo-CoP-160. Otherwise, as described in Table S3, Mo-CoP possesses much lower charge-transfer resistance (0.66Ω) than Mo-CoP-120 (1.02Ω) and Mo-CoP-160 (1.39Ω). In addition, the reaction temperature during the second synthetic step plays an important role in the electrocatalytic OER activity. As shown in Figure S25a,

the Mo-CoP obtained at 140°C exhibits the lowest overpotential at 100 mA/cm^2 compared to Mo-CoP-120 and Mo-CoP-160. Moreover, as shown in Figure S25b, the Tafel slope of Mo-CoP obtained at 140°C is lower than that

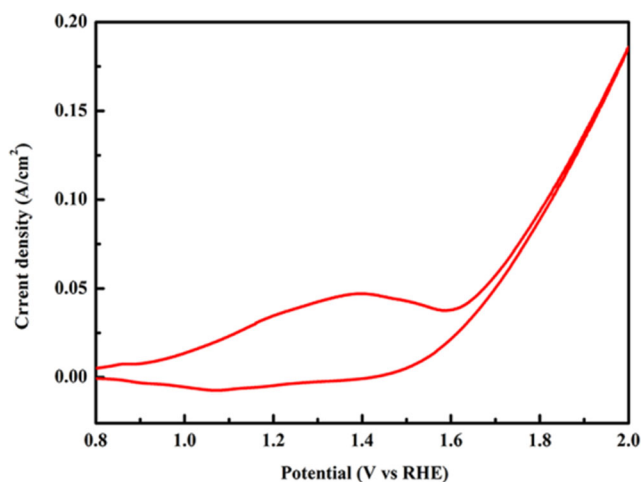


Fig. 6 CV curve of an alkaline electrolyzer using Mo-CoP||Mo-CoP as two electrodes in 1 M KOH with a scan rate of 1 mV/s

of Mo-CoP-120 and Mo-CoP-160. As shown in the SEM images in Figure S26, the Mo-CoP obtained at 140 °C has a larger active surface. In summary, 140 °C should be the most reasonable reaction temperature.

Inspired by the outstanding catalytic activity of Mo-CoP toward both HER and OER, we further investigated its potential application via employing it as both anode and cathode for over water splitting. The catalytic activity of Mo-CoP was measured by CV at a scan rate of 1 mV/s. we can learn from Fig. 6 that the Mo-CoP||Mo-CoP electrode couple exhibit superior properties with an onset potential of 1.42 V and deliver a 10 mA/cm² with a voltage value of only 1.54 V, which outperforms that of the Pt/C/NF||RuO₂ NPs/NF water electrolyzer (1.61 V)[50]. The voltage value also lower than those of the recently reported water electrolyzers (Table S5). In addition, the performance of the catalyst is still outstanding at higher current densities. This water electrolyzer displays superior performance that requires a cell voltage of 1.59, 1.70, and 1.82 V to provide 20, 50, and 100 mA/cm² water splitting current in 1.0 M KOH respectively. But it is a pity that after the water splitting, the morphology of the cathode and anode was damaged to varying degrees (Figure S27). Therefore, there still a long way to go to improve the performance of this catalyst to meet the need of a practical application.

Conclusions

In this report, Mo-CoP, an electrocatalyst with high performance for HER, was successfully prepared by the development of CoCO on NF via hydrothermal processes and thermal treatment method. For shortening the charge diffusion path, the catalyst is made into nanosheets. The surface area of the rough nanosheets obtained after phosphating is further increased. The incorporation of Mo could enlarge the electrochemically active surface area of the catalyst and adjust the electronic structure of Co. And the intimate contact between Mo-CoP nanosheets and NF fastens the electron transport. Mo-CoP has improved OER (η_{10} =235 mV) and HER (η_{10} =47 mV, η_{100} =114 mV) bifunctionality. Moreover, Mo-CoP||Mo-CoP electrode couple exhibit superior properties as well. This work offers a facile and practicable method for the development of effective and low-cost electrocatalysts for HER and OER and will open up a promising avenue toward exploring the design of catalysts.

Supplementary Information The online version contains supplementary material available at <https://doi.org/10.1007/s11581-021-04071-4>.

Funding This work was financially supported by the National Natural Science Foundation of China (51674221 and 51704261) and the Natural Science Foundation of Hebei Province (B2018203330 and B2018203360).

References

- Li Y, Huang H, Chen S, Wang C, Liu A, Ma T (2018) Catal Lett 149:486–495
- Zhang J, Wang T, Liu P, Liao Z, Liu S, Zhuang X, Chen M, Zschech E, Feng X (2017) Efficient hydrogen production on MoNi₄ electrocatalysts with fast water dissociation kinetics. Nat Commun 8:15437
- Zhai P, Zhang Y, Wu Y, Gao J, Zhang B, Cao S, Zhang Y, Li Z, Sun L, Hou J (2020) Engineering active sites on hierarchical transition bimetal oxides/sulfides heterostructure array enabling robust overall water splitting. Nat Commun 11:5462
- Du J, Wang L, Bai L, Dang S, Su L, Qin X, Shao G, Colloid Interface J (2019) Sci. 535:75–83
- Xiong Q, Wang Y, Liu P-F, Zheng L-R, Wang G, Yang H-G, Wong P-K, Zhang H, Zhao H (2018) Cobalt Covalent Doping in MoS₂ to Induce Bifunctionality of Overall Water Splitting. Adv Mater 30:1801450
- Wang X, Tong R, Wang Y, Tao H, Zhang Z, Wang H (2016) Surface Roughening of Nickel Cobalt Phosphide Nanowire Arrays/Ni Foam for Enhanced Hydrogen Evolution Activity. ACS Appl Mater Interfaces 8:34270–34279
- Pu Z, Zhao J, Amiin IS, Li W, Wang M, He D, Mu S (2019) A universal synthesis strategy for P-rich noble metal diphosphide-based electrocatalysts for the hydrogen evolution reaction. Energy Environ Sci 12:952–957
- Zhou W, Huang D-D, Wu Y-P, Zhao J, Wu T, Zhang J, Li D-S, Sun C, Feng P, Bu X (2019) Stable Hierarchical Bimetal-Organic Nanostructures as High-Performance Electrocatalysts for the Oxygen Evolution Reaction. Angew Chem Int Ed 58:4227–4231
- Baek M, Kim G-W, Park T, Yong K (2019) NiMoFe and NiMoFeP as Complementary Electrocatalysts for Efficient Overall Water Splitting and Their Application in PV-Electrolysis with STH 12.3%. Small 15:1905501
- Lv L, Yang Z, Chen K, Wang C, Xiong Y (2019) 2D Layered Double Hydroxides for Oxygen Evolution Reaction: From Fundamental Design to Application. Adv Energy Mater 9:1803358
- Cai Z, Bu X, Wang P, Ho JC, Yang J, Wang X, Mater J (2019) Chem A 7:5069–5089
- Huang C-L, Chuah X-F, Hsieh C-T, Lu S-Y (2019) NiFe Alloy Nanotube Arrays as Highly Efficient Bifunctional Electrocatalysts for Overall Water Splitting at High Current Densities. ACS Appl Mater Interfaces 11:24096–24106
- Ganesan P, Sivanantham A, Shanmugam S (2017) Nanostructured Nickel–Cobalt–Titanium Alloy Grown on Titanium Substrate as Efficient Electrocatalyst for Alkaline Water Electrolysis. ACS Appl Mater Interfaces 9:12416–12426
- Hu EL, Feng YF, Nai JW, Zhao D, Hu Y, Lou XW (2018) Construction of hierarchical Ni–Co–P hollow nanobricks with oriented nanosheets for efficient overall water splitting. Energy Environ Sci 11:872–880
- Dang Y, He J, Wu T, Yu L, Kerns P, Wen L, Ouyang J, Suib SL (2019) Constructing Bifunctional 3D Holey and Ultrathin CoP Nanosheets for Efficient Overall Water Splitting. ACS Appl Mater Interfaces 11:29879–29887
- Cui Z, Ge Y, Chu H, Baines R, Dong P, Tang J, Yang Y, Ajayan PM, Ye M, Shen J, Mater J (2017) Chem A 5:1595–1602
- Hang L, Zhang T, Sun Y, Men D, Lyu X, Zhang Q, Cai W, Li Y, Mater J (2018) Chem A 6:19555–19562
- Wang Y, Sun Y, Yan F, Zhu C, Gao P, Zhang X, Chen Y, Mater J (2018) Chem A 6:8479–8487
- Huang C, Ouyang T, Zou Y, Li N, Liu Z-Q, Mater J (2018) Chem A 6:7420–7427
- Ai L, Su J, Wang M, Jiang J (2018) Bamboo-Structured Nitrogen-Doped Carbon Nanotube Coencapsulating Cobalt and

- Molybdenum Carbide Nanoparticles: An Efficient Bifunctional Electrocatalyst for Overall Water Splitting. *ACS Sustain Chem Eng* 6:9912–9920
21. Xue Z-H, Su H, Yu Q-Y, Zhang B, Wang H-H, Li X-H, Chen J-S (2017) Janus Co/CoP Nanoparticles as Efficient Mott-Schottky Electrocatalysts for Overall Water Splitting in Wide pH Range. *Adv Energy Mater* 7:1602355
 22. Li Y, Jia B, Chen B, Liu Q, Cai M, Xue Z, Fan Y, Wang H-P, Su C-Y, Li G (2018) MOF-derived Mn doped porous CoP nanosheets as efficient and stable bifunctional electrocatalysts for water splitting. *Dalton Trans* 47:14679–14685
 23. Zhang M, Ci S, Li H, Cai P, Xu H, Wen Z (2017) Highly defective porous CoP nanowire as electrocatalyst for full water splitting. *Int J Hydrog Energy* 42:29080–29090
 24. Du H, Liu Q, Cheng N, Asiri AM, Sun X, Li CM, Mater J (2014) *Chem A* 2:14812–14816
 25. Liu T, Xie L, Yang J, Kong R, Du G, Asiri AM, Sun X, Chen L (2017) Self-Standing CoP Nanosheets Array: A Three-Dimensional Bifunctional Catalyst Electrode for Overall Water Splitting in both Neutral and Alkaline Media. *ChemElectroChem* 4:1840–1845
 26. Zhang R, Tang C, Kong R, Du G, Asiri AM, Chen L, Sun X (2017) Al-Doped CoP nanoarray: a durable water-splitting electrocatalyst with superhigh activity. *Nanoscale* 9:4793–4800
 27. Liu X, Wei B, Su R, Zhao C, Dai D, Ma X, Xu L (2019) Mo-Doped Cobalt Phosphide Nanosheets for Efficient Hydrogen Generation in an Alkaline Media. *Energy Technology* 7:1900021
 28. Liu Z, Yu X, Xue H, Feng L, Mater J (2019) *Chem A* 7:13242–13248
 29. Yi T-F, Pan J-J, Wei T-T, Li Y, Cao G (2020) NiCo₂S₄-based nanocomposites for energy storage in supercapacitors and batteries. *Nano Today* 33:100894
 30. Yi TF, Qu JP, Lai X, Han X, Chang H, Zhu YR (2021) Toward high-performance Li storage anodes: design and construction of spherical carbon-coated CoNiO₂ materials. *Materials Today Chemistry* 19:100407
 31. Yi T-F, Chang H, Wei T-T, Qi S-Y, Li Y, Zhu Y-R (2021) Approaching high-performance electrode materials of ZnCo₂S₄ nanoparticle wrapped carbon nanotubes for supercapacitors. *J Mater* 7:563–576
 32. Yi T-F, Qiu L-Y, Mei J, Qi S-Y, Cui P, Luo S, Zhu Y-R, Xie Y, He Y-B (2020) Porous spherical NiO@NiMoO₄@PPy nanoarchitectures as advanced electrochemical pseudocapacitor materials. *Sci Bull* 65:546–556
 33. Huang X, Xu X, Luan X, Cheng D (2020) CoP nanowires coupled with CoMoP nanosheets as a highly efficient cooperative catalyst for hydrogen evolution reaction. *Nano Energy* 68:104332
 34. Han L, Yu TW, Lei W, Liu WW, Feng K, Ding YL, Jiang GP, Xu P, Chen ZW, Mater J (2017) *Chem A* 5:16568–16572
 35. Hao J, Yang W, Zhang Z, Tang J (2015) Metal-organic frameworks derived CoxFe1-xP nanocubes for electrochemical hydrogen evolution. *Nanoscale* 7:11055–11062
 36. Li Y, Liu J, Chen C, Zhang X, Chen J (2017) Preparation of NiCoP Hollow Quasi-Polyhedra and Their Electrocatalytic Properties for Hydrogen Evolution in Alkaline Solution. *ACS Appl Mater Interfaces* 9:5982–5991
 37. Li Y, Niu S, Rakov D, Wang Y, Caban-Acevedo M, Zheng S, Song B, Xu P (2018) Metal organic framework-derived CoPS/N-doped carbon for efficient electrocatalytic hydrogen evolution. *Nanoscale* 10:7291–7297
 38. Pan Y, Sun K, Liu S, Cao X, Wu K, Cheong W-C, Chen Z, Wang Y, Li Y, Liu Y, Wang D, Peng Q, Chen C, Li Y (2018) Core-Shell ZIF-8@ZIF-67-Derived CoP Nanoparticle-Embedded N-Doped Carbon Nanotube Hollow Polyhedron for Efficient Overall Water Splitting. *J Am Chem Soc* 140:2610–2618
 39. Weng BC, Wei W, Yiliguma, Wu H, Alenizi AM, Zheng GF (2016) *J Mater Chem A* 4:15353–15360
 40. Yang FL, Chen YT, Cheng GZ, Chen SL, Luo W (2017) Ultrathin Nitrogen-Doped Carbon Coated with CoP for Efficient Hydrogen Evolution. *ACS Catal* 7:3824–3831
 41. Yu SH, Chua DHC (2018) Toward High-Performance and Low-Cost Hydrogen Evolution Reaction Electrocatalysts: Nanostructuring Cobalt Phosphide (CoP) Particles on Carbon Fiber Paper. *ACS Appl Mater Interfaces* 10:14777–14785
 42. Chen D, Zhu J, Mu X, Cheng R, Li W, Liu S, Pu Z, Lin C, Mu S (2020) Nitrogen-Doped carbon coupled FeNi₃ intermetallic compound as advanced bifunctional electrocatalyst for OER, ORR and zn-air batteries. *Appl Catal B* 268:118729
 43. Chu W, Shi Z, Hou Y, Ma D, Bai X, Gao Y, Yang N (2020) Trifunctional of Phosphorus-Doped NiCo₂O₄Nanowire Materials for Asymmetric Supercapacitor, Oxygen Evolution Reaction, and Hydrogen Evolution Reaction. *ACS Appl Mater Interfaces* 12:2763–2772
 44. Gong Y, Yang Z, Lin Y, Wang J, Pan H, Xu Z, Mater J (2018) *Chem A* 6:16950–16958
 45. Hu K, Wu M, Hinokuma S, Ohto T, Wakisaka M, Fujita J-i, Ito Y, Mater J (2019) *Chem A* 7:2156–2164
 46. Lai C, Liu X, Wang Y, Cao C, Yin Y, Yang H, Qi X, Zhong S, Hou X, Liang T (2020) Modulating ternary Mo–Ni–P by electronic re-configuration and morphology engineering for boosting all-pH electrocatalytic overall water splitting. *Electrochim Acta* 330:135294
 47. Wang Z, Liu H, Ge R, Ren X, Ren J, Yang D, Zhang L, Sun X (2018) Phosphorus-Doped Co₃O₄Nanowire Array: A Highly Efficient Bifunctional Electrocatalyst for Overall Water Splitting. *ACS Catal* 8:2236–2241
 48. Yan H, Xie Y, Wu A, Cai Z, Wang L, Tian C, Zhang X, Fu H (2019) Anion-Modulated HER and OER Activities of 3D Ni–V-Based Interstitial Compound Heterojunctions for High-Efficiency and Stable Overall Water Splitting. *Adv Mater* 31:1901174
 49. Zhang Y, Shao Q, Long S, Huang X (2018) Cobalt-molybdenum nanosheet arrays as highly efficient and stable earth-abundant electrocatalysts for overall water splitting. *Nano Energy* 45:448–455
 50. Li Y, Li F, Zhao Y, Li S-N, Zeng J-H, Yao H-C, Chen Y, Mater J (2019) *Chem A* 7:20658–20666

Publisher's note Springer Nature remains neutral with regard to jurisdictional claims in published maps and institutional affiliations.